

Synthetic Time Series Generation via Complex Networks*

Jaime Vale¹, Vanessa Freitas Silva^{1,2}, Maria Eduarda Silva^{1,2}, and Fernando Silva^{3,4}

¹Faculdade de Ciências, Universidade do Porto

²INESC TEC-CRACS

³Faculdade de Economia, Universidade do Porto

⁴INESC TEC-LIAAD

Abstract

Time series data are essential for a wide range of applications, particularly in developing robust machine learning models. However, access to high-quality datasets is often limited due to privacy concerns, acquisition costs, and labeling challenges. Synthetic time series generation has emerged as a promising solution to address these constraints. In this work, we present a framework for generating synthetic time series by leveraging complex networks mappings. Specifically, we investigate whether time series transformed into Quantile Graphs (QG) – and then reconstructed via inverse mapping – can produce synthetic data that preserve the statistical and structural properties of the original. We evaluate the fidelity and utility of the generated data using both simulated and real-world datasets, and compare our approach against state-of-the-art Generative Adversarial Network (GAN) methods. Results indicate that our quantile graph-based methodology offers a competitive and interpretable alternative for synthetic time series generation.

Keywords: synthetic time series, complex networks, time series mappings, quantile graph, network-based generation

1 Introduction

Time series data are ubiquitous across all domains, ranging from production line records [Halder and Newe, 2022], physiological measurements [Chowdhury et al., 2019], electrical readings [Leukam Lako et al., 2021] to trajectory tracking [Roman, 2023], often exhibiting unique and complex temporal dependencies. However, data shortage due to privacy concerns, limited accessibility, cost and opportunity of large-scale data collection, hinder the development of appropriate and robust methods and models. To address these limitations, synthetic time series generation has emerged as a powerful solution [Lin et al., 2020]. Synthetic time series data can be defined as artificially generated datasets that replicate the statistical and dynamical properties of real-world data [Pezoulas et al., 2024], enabling robust machine learning models development, benchmarking, and exploratory analysis without relying on sensitive or scarce data. Yet, a key challenge remains: ensuring that synthetic data maintains fidelity – preserving statistical and dynamic characteristics (e.g., autocorrelation, trends, linearity, and heterogeneity) – and utility – remaining useful for downstream tasks like clustering, classification or forecasting.

Innovative approaches based on Generative Adversarial Networks (GANs) [Lin et al., 2020, Brophy et al., 2023, Yoon et al., 2019] are among the most effective and widely used techniques today for synthetic time series generation due to their ability to model complex distributions. However, GAN-based methods often

*Submitted authors manuscript in International Journal of Data Science and Analytics on October 19, 2025. CONTACT Vanessa Freitas Silva. Email: vanessa.silva@fc.up.pt

suffer from instability during training, lack interpretability, and require extensive hyperparameter tuning, which can hinder their practical deployment [Iglesias et al., 2023].

In this work, we aim to contribute to the literature on synthetic time series generation by presenting an alternative framework to synthesizing time series data using complex network mappings. Specifically, we leverage the principles of network science to transform time series into graphs that encapsulate their structural and temporal properties. Prior research has shown that such mappings can effectively capture key dynamics [Silva et al., 2021, Silva et al., 2022] and have been successfully applied to tasks like classification [Campanharo et al., 2020], clustering [Silva et al., 2022], outlier detection [Hu et al., 2020], and forecasting [Huang et al., 2021]. While most time series-to-network mappings are not reversible – meaning the exact original time series cannot be recovered from the resulting graph [Lacasa et al., 2008] – probability transition methods such as the *Quantile Graph* [Campanharo et al., 2011] allow for inverse mappings, thus enabling the generation of a new time series with similar properties to the original.

Building on this premise, we propose and assess a methodology that combines *Quantile Graph* and *Inverse Quantile Graph* mappings to synthesize time series data. In a nutshell, time series data are transformed into graphs via quantile mappings and then reconstructed using a reverse mapping algorithm. This approach enables the generation of sets of synthetic time series that statistically resemble the original data. We evaluate the fidelity and utility of the generated synthetic data using both statistical metrics and network topological features. Experimental analysis indicates that the synthetic time series preserves key statistical and dynamic properties, while remaining useful for downstream tasks. To validate our approach, we conduct experiments using both time series from controlled settings (generated from well-known time series models) and real datasets. We compare our methodology against state-of-the-art GAN-based frameworks, including *TimeGAN* [Yoon et al., 2019] and *DoppelGANger* [Lin et al., 2019], demonstrating its effectiveness through qualitative analysis on both simulated and real-world datasets.

Compared to GAN-based methods, our approach produce superior fidelity, greater interpretability, reduced need for parameter tuning (it has only one parameter, the number of quantiles), and improved computational efficiency (no need for training).

The paper is organized as follows. Section 2 provides the background and introduces key terminology, including the time series mapping methods, relevant to this work. It also reviews related work in synthetic time series generation. Section 3 presents the proposed methodology. We begin by formulating the problem and then introduce the *Inverse Quantile Graph* mapping technique, detailing how it complements the forward quantile mapping to enable synthetic data generation. Section 4 describes the empirical evaluation. We outline the experimental workflow, including the simulated and real dataset used, and assess the fidelity and utility of the synthetic time series using statistical and topological features. This section also includes a comparative analysis against benchmark GAN-based methods. Finally, Section 5, summarizes the main findings and indicates future directions.

2 Background and Related Work

In this section, we introduce the fundamental concepts and terminology for the remainder of this document. We start by reviewing related work in time series synthesizing methods. Then, we provide a detailed description of the mapping methods employed in this work, namely the *Quantile Graph* (*QG*) mapping and its inverse [Campanharo et al., 2011].

2.1 Time Series Data Synthesizing and Augmenting Methods

Time series data generation is not a novel concept but has gained traction in theory and practice as a promising solution to data shortages and limitations that hinder processing and extracting meaningful insights from the data [Asghar et al., 2017, Shi et al., 2011, Benhamouda et al., 2016] and training deep learning models effectively [Iglesias et al., 2023, Iwana and Uchida, 2021, Wen et al., 2021].

Data Augmentation is the process of modifying or creating new data by adding noise, performing permutations and by generating new synthetic data, all while preserving original data characteristics. In augmentation-related transformations, methods include manipulation techniques based on deformation, shortening, enlargement, and data modification [Iglesias et al., 2023]. For example, *time slicing* involves cutting portions of data (windows) to create new samples, *jittering* adds noise to simulate inherent data variability, *scaling* modifies the magnitude of observations, either uniformly (homogeneous scaling) or variably at specific points (magnitude warping), *rotation* transforms time series data by applying a rotation matrix (converted from original time series) to represent it in a new orientation, *permutation* rearranges fixed or variable-length window segments of a time series to create new combinations, and *channel permutation*, applied to multivariate time series, swaps the positions of features (channels) to expand the dataset [Iwana and Uchida, 2021, Iglesias et al., 2023]. Traditional methods rely on imputation and statistical approaches. These typically involve applying mathematical expressions or perform a series of transformations to modify the data or simulate new samples in order to complete or augment the dataset [Kloppies and Schwung, 2024]. Early approaches make use of simple interpolation techniques (such as linear and spline interpolation), regression models, and machine learning-based methods like K-Nearest Neighbors (KNN).

Simulations or modeling are also often employed to replicate real-world scenarios when data is scarce. Examples include autoregressive models, such as mixture autoregressive (MAR) [Kang et al., 2020], Markov chains [Negra et al., 2008], and seasonal-trend decomposition (STL)-based techniques [Kegel et al., 2018]. Although these methods are useful, they often lack diversity and quality, and fail to model or simulate complex temporal dynamics and feature interactions [Kloppies and Schwung, 2024]. An emerging solution that is gaining increasing attention is the generation of synthetic time series that replicate the statistical and dynamic properties of the original datasets. Recent techniques based on deep-learning methods have been proposed for this purpose, including *Generative Adversarial Networks* (GANs) [Lin et al., 2020, Brophy et al., 2023, Yoon et al., 2019] and *Variational Autoencoders* (VAEs) [Iglesias et al., 2023, Hu et al., 2020]. VAE-based methods [Kingma et al., 2013] employ probabilistic latent variable models to learn the underlying distribution of time series data, enabling the generation of new data by sampling from the learned latent space [Hu et al., 2020]. Although VAEs are effective for synthetic data generation, their use has become less prevalent with the advent of newer neural network models, such as GANs, which can produce larger and more diverse datasets. Nevertheless, VAEs remain valuable in scenarios that require precise control over the variability of generated data, maintaining their relevance in specific domains [Iglesias et al., 2023]. GANs are powerful tools for synthesizing high-quality, diversified, and privacy-preserving time series data. GANs not only generate synthetic datasets but also support tasks such as data augmentation, denoising, and imputing missing values [Brophy et al., 2023, Gao et al., 2022].

A standard GAN consists of two neural networks: the generator that creates synthetic data instances, aiming to mimic the original data; and the discriminator that evaluates whether a given data instance is real or synthetic. These networks are trained jointly using a zero-sum adversarial framework, where the generator improves by learning to "fool" the discriminator, and the discriminator evolves to better distinguish real from synthetic data. Despite their success, traditional GANs often struggle to preserve the temporal dependencies inherent to time series data [Brophy et al., 2023, Gao et al., 2022, Yoon et al., 2019].

To address these limitations, specialized GAN architectures have been developed. Some more recent examples include: *Recurrent Conditional GAN* (RCGAN) that focuses on recurrent structures to better capture sequential relationships [Hyland et al., 2018]; *TimeGAN* that introduces a supervised loss function and an embedding network to better capture temporal dynamics and conditional distributions in time series data [Yoon et al., 2019]; and *DoppelGANger* that enhances scalability and utility for complex time series by introducing conditional inputs and auxiliary variables [Lin et al., 2019]. Despite their strengths, GANs face several challenges. Training instability is a common issue due to the adversarial nature of the model, often leading to mode collapse, where the generator produces limited variations and repetitive outputs of data. Furthermore, achieving convergence is difficult, as the generator and discriminator must reach a balance, which may not always occur in practice. Additionally, GANs are computationally expensive, requiring significant resources for effective training. Applying GANs to large-scale datasets or high-resolution time series often amplifies these challenges, requiring architectural innovations or alternative frameworks [Brophy et al., 2023, Iglesias et al., 2023]. These limitations hinder the widespread application of GANs and imply careful tuning and domain-specific adjustments for a successful implementation.

In all the approaches aimed at generating more data maintaining data utility remains a major concern.

2.2 Mapping Time Series into Quantile Graphs

Time series analysis using network science involves mapping time series data (\mathbf{Y}) into complex networks (graphs, G), composed of nodes (V) and edges (E). Nodes represent specific time points or temporal patterns, while edges capture temporal dependencies or relationships between pairs of nodes. Common mapping approaches rely on principles such as visibility, probability transition, proximity, and statistical principles [Silva et al., 2021]. In this work, we focus on the probability transition approach.

Transition probability mappings capture temporal dynamics from the original data and encode them into an adjacency matrix that defines the resulting graph. In particular, the *Quantile Graph* (QG) [Campanharo et al., 2011] applies this approach by representing a time series $\mathbf{Y} = \{Y_t\}_{t=1}^T$ as a directed and weighted graph G obtained from the following steps (see Algorithm 1 in Appendix A):

Step 1: split the support of the time series into \mathcal{Q} sample quantiles, $\{q_1, q_2, \dots, q_{\mathcal{Q}}\}$.

Step 2: map each quantile, q_i , into a node $v_i \in V$ in the graph G .

Step 3: link two nodes, v_i and v_j , with a directed and weighted edge, $(v_i, v_j, w_{i,j}) \in E$, based on how often the time series transitions between their corresponding quantiles q_i and q_j , in the time series. The weight $w_{i,j}$ represents the number of times a data point Y_t in quantile q_i is followed by Y_{t+1} in quantile q_j .

Step 4: normalize the adjacency matrix of G into a Markov transition matrix, \mathbf{W} , where $\sum_{j=1}^{\mathcal{Q}} w_{i,j} = 1$, for each $i = 1, \dots, \mathcal{Q}$, where the weight $w_{i,j}$ represents the transition probability between the corresponding quantile samples.

Figure 1 illustrates the QG mapping method.

Campanharo et al. in [Campanharo et al., 2011] introduced an inverse mapping function for the QG described above enabling the generation of a new time series \mathbf{Y}^* from an existing quantile graph G that represents the original series \mathbf{Y} . This mapping leverages the Markov transition matrix \mathbf{W} , associated to G 's adjacency matrix, to reconstruct \mathbf{Y} .

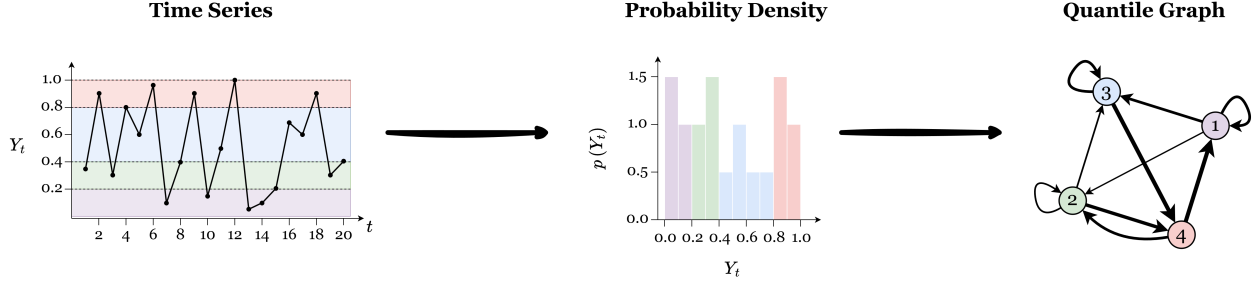


Figure 1: Illustration of Quantile Graph mapping method with a toy time series. *Source:* Adapted from [Campanharo et al., 2011, Silva et al., 2021].

The extension of this inverse QG mapping to synthesize time series that preserve utility and fidelity is described in detail in the following section.

3 Synthetic Time Series via Quantile Graphs

Let $\mathbf{Y} = \{Y_1, Y_2, \dots, Y_T\}$ represent a time series of T sequential observations. The goal is to generate synthetic time series $\mathbf{Y}^* = \{Y_1^*, Y_2^*, \dots, Y_T^*\}$, such that \mathbf{Y}^* retains the key statistical, structural and dynamic properties of \mathbf{Y} , fidelity preservation and the analysis of \mathbf{Y}^* is meaningful in addressing particular tasks related to \mathbf{Y} , i.e., utility preservation.

We introduce a 2-step approach:

1. **Network-Domain Mapping:** Introduce a forward mapping $\mathcal{M} : \mathcal{T} \rightarrow \mathcal{G}$, which uses transition probabilities to transform a time series $\mathbf{Y} \in \mathcal{T}$ into a graph $G = (V, E, \mathbf{W}) \in \mathcal{G}$.
2. **Time-Series Reverse Mapping (Reconstruction):** Define an inverse mapping $\mathcal{M}^{-1} : \mathcal{G} \rightarrow \mathcal{T}$, to reconstruct a synthetic series $\mathbf{Y}^* \in \mathcal{T}$ from the Markov transition matrix \mathbf{W} representing graph G .

Focusing on quantile-based mappings, our approach, *Inverse Quantile Graph (InvQG)* henceforward, is illustrated in Figure 2.

InvQG mapping involves the following steps (see Algorithm 2 in Appendix A):

Step 1: Extract the adjacency (Markov transition) matrix \mathbf{W} of the quantile graph produced by QG mapping (line 2).

Step 2: Retrieve the sample quantiles of the original time series (line 2).

Step 3: Select an initial quantile q_k at random among those with nonzero outgoing probability (line 5).

Step 4: For $t = 1, \dots, T$:

Step 4.1: Determine the value range of the current quantile q_k (lines 7–8).

Step 4.2: Sample a value uniformly from that range (line 9).

Step 4.3: Transition to the next quantile $q_{k'}$ by sampling according to the nonzero probabilities in row k of \mathbf{W} (line 10).

Step 5: Return a synthetic time series data (line 12).

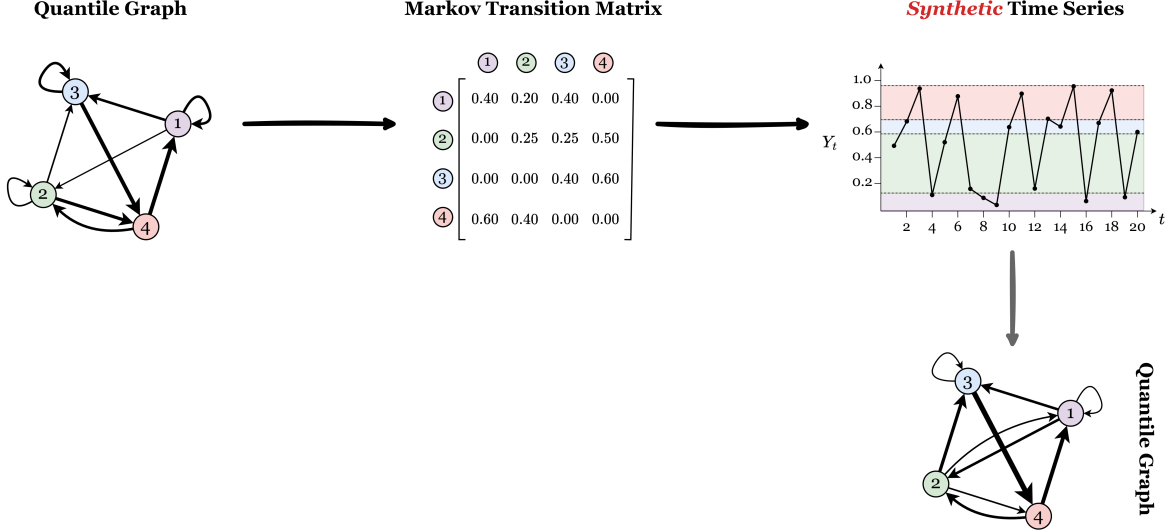


Figure 2: Illustration of the Inverse Quantile Graph (*InvQG*) mapping method, including the quantile graph derived from the synthetic time series. *Source*: Adapted from [Campanharo et al., 2011].

An important advantage of this synthetic time series generation method is its ability to produce multiple distinct realizations that preserve the original data’s dynamic and statistical characteristics. This diversity arises from the probabilistic elements in Algorithm 2: the Markov transition matrix governs the selection of each quantile q_i , and each value Y_t is sampled uniformly between the lower and upper bounds of the chosen quantile. By generating a richer ensemble of series, we can augment the dataset and thereby enhance the robustness and accuracy of downstream analytical tasks.

The code of the *QG* and *InvQG* algorithms are available on GitHub: <https://github.com/vanessa-silva/InvQG>.

4 Empirical Evaluation

This section evaluates the fidelity and utility of synthetic data generated by our Inverse Quantile Graph (*InvQG*) method, focusing on the preservation of key properties from the original time series. We begin with a large, diverse collection of series simulated from established statistical models, which serve as the ground truth. We then assess how well *InvQG* reproduces these properties using:

- **Statistical measures** that capture temporal dynamics (e.g., autocorrelation, linearity, and distributional characteristics).
- **Topological metrics** derived from the time-series-graph representation (e.g., degree, clustering coefficient, and path lengths).

Next, we benchmark *InvQG* against two state-of-the-art generative models: *TimeGAN* [Yoon et al., 2019] and *DoppelGANger* [Lin et al., 2019], comparing their ability to preserve data distribution properties. Finally, we evaluate the utility of the synthetic time series in a clustering task.

To contextualize our evaluation, we first outline the adopted methodology and describe the datasets used in our experiments.

4.1 Methodology

The methodology employed in this study is summarized by the flow diagram shown in Figure 3.

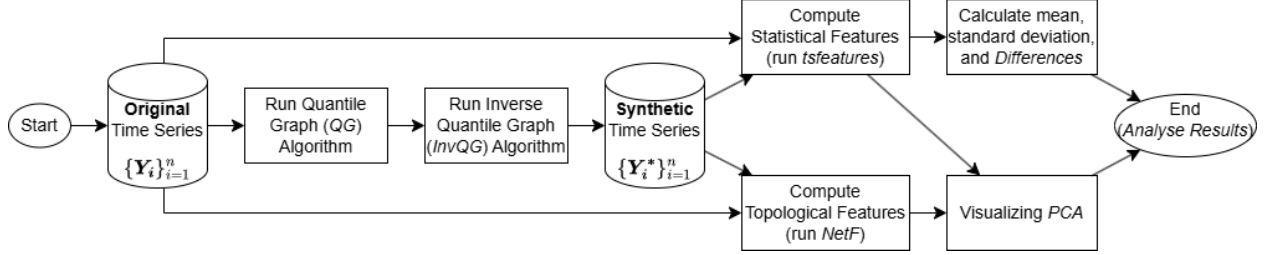


Figure 3: Diagram of the methodology implemented in this work.

For each time series Y_i in a set of n time series $\{Y_i\}_{i=1}^n$, we generate a synthetic time series $\{Y_i^*\}_{i=1}^n$ applying QG (Algorithm 1) and then *InvQG* (Algorithm 2) mappings. Then, we extracted two sets of features: statistical features, *tsfeatures* available in the R package [Hyndman et al., 2023], and topological features in the domain of complex networks, *NetF* [Silva et al., 2022]¹, from both the original Y_i and synthetic Y_i^* data, and we analyse them as paired samples.

For reproducibility purposes, the source code and the datasets are made available in <https://github.com/vanessa-silva/InvQG>.

4.2 Datasets

To evaluate the proposed methodology, we employed two distinct types of time series datasets: 1) the *artificiality dataset*, consisting of simulated time series models designed to provide a controlled environment for analysing; and 2) the *real dataset*, composing actual smart meter readings that reflect real usage patterns and variability.

In the following sections, we describe both time series datasets in more detail.

4.2.1 Artificial Dataset

To control for relevant time series characteristics we generated original time series from eleven well-known statistical time series models, summarized in Table 1. Further details can be found at [Silva et al., 2022]. The full artificial data set consists of $n = 100$ time series of length $T = 10000$ for each statistical model, for a total of 1100 time series. We will refer to this dataset as an *artificial dataset*.

4.2.2 Real Dataset

We also utilize an energy dataset containing domestic consumption measurements from the East Midlands, UK [Richardson and Thomson, 2010]². The dataset comprises smart meter readings from twenty-two different households, with a sampling frequency of one minute over two years (2008 and 2009). Each household exhibits a unique consumption pattern, providing sufficient behavioural diversity to pose a meaningful challenge for synthesizing data and enabling robust comparative analysis. We will refer to this dataset as a *real dataset*.

¹ Available at <https://github.com/vanessa-silva/NetF>

² Available at <https://beta.ukdataservice.ac.uk/datacatalogue/studies/study?id=6583>

Table 1: Statistical time series models for the artificial dataset.

Model	Parameters	Main Property	Notation
White Noise	$\epsilon_t \sim N(0, 1)$	Noise effect	WN
AR(1)	$\phi_1 = -0.5$ $\phi_1 = 0.5$ $\phi_1 = 0.9$	Smooth oscillation Moderate persistence High persistence	AR1 -0.5 AR1 0.5 AR1 0.9
AR(2)	$\phi_1 = 1.5, \phi_2 = -0.75$	Pseudo-periodic	AR2
ARIMA(1, 1, 0)	$\phi_1 = 0.7$	Stochastic trend	ARIMA
ARFIMA(1, 0.4, 0)	$\phi_1 = 0.9$	Long memory effect	ARFIMA
GARCH(1, 1)	$\omega = 10^{-6}, \alpha_1 = 0.1, \beta_1 = 0.8$	Persistent periods of high or low volatility	GARCH
SETAR(1)	$\alpha = 0.5, \beta = -1.8, \gamma = 2, r = -1$	Regime-dependent autocorrelation	SETAR
Poisson-HMM	$N = 2, \begin{bmatrix} 0.9 & 0.1 \\ 0.1 & 0.9 \end{bmatrix} \lambda \in \{10, 15\}$	State transitions	HMM
INAR(1)	$\alpha = 0.5, \epsilon_t \sim Po(1)$	Correlated counts	INAR

The preprocessing steps applied to the real dataset are outlined below:

- **Missing Data Handling:** The largest time series has a length of $T = 1052640$, but some of the 22 time series are shorter ($T < 1052640$, with durations of less than one or two years), resulting in a dataset with time series length varying in $T \in [264331, 1052640]$. Furthermore, all time series instances contain missing values, where the percentage of missing values varying between 0.02% and 33.47%. To address this, we applied the *InvQG* method for imputation, since traditional imputation techniques often perform poorly on this type of data, and using *InvQG* not only improves the imputations but also demonstrates the versatility of the quantile-based approach.
- **Time Aggregation:** Due to the high temporal resolution of the original data (one-minute intervals), we aggregated the time series to an hourly frequency. This results in hourly consumption profiles of length $T \in [4406, 17544]$ observations. While the *InvQG* method is not constrained by time resolution, that is, the method does not have runtime limitations, this aggregation was necessary to accommodate the computational limitations associated with GAN-based methods when processing high-resolution data.

4.3 Fidelity Analysis via Statistical Features

In this section, we analyse the fidelity of quantile-based mappings for synthetic time series data generation. We conduct an in-depth comparative analysis of the main statistical properties between the original time series data and their synthetic counterparts. This analysis is performed on the artificial dataset (in a controlled and interpretable setting), using the popular R package *tsfeatures* to extract statistical features from the series.

Figures 4 and 5 represent boxplots for the paired samples (*synthetic - original*) of *tsfeatures* [Hyndman et al., 2023]. Table 3, in appendix, present the corresponding mean and standard deviation of the sample differences.

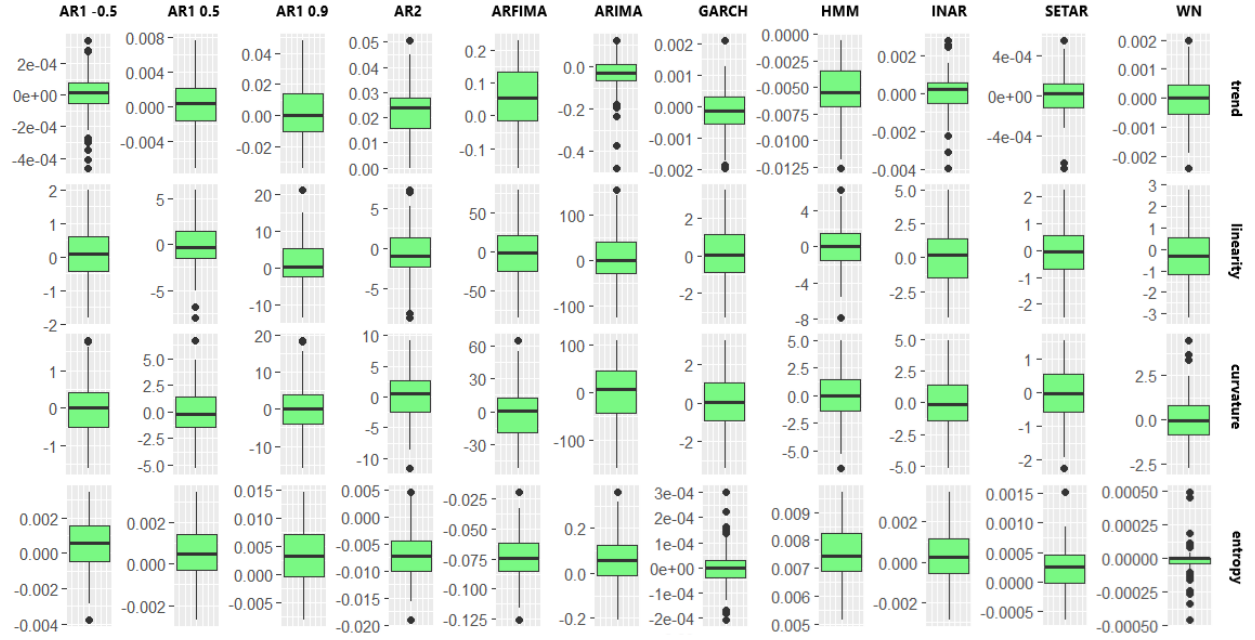


Figure 4: Boxplots of the paired samples statistical features: *trend*, *linearity*, *curvature* and *entropy* (synthetic - original).

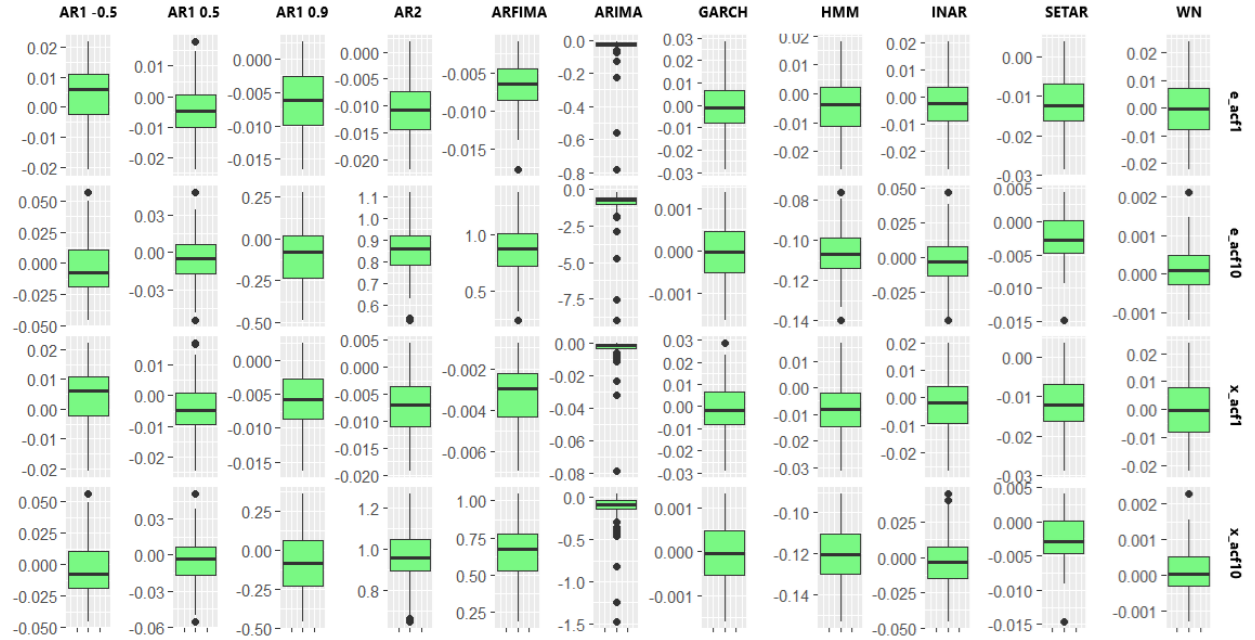


Figure 5: Boxplots of the paired samples statistical features: *e_acf1*, *e_acf10*, *x_acf1* and *x_acf10* (synthetic - original).

In general, we observe that the median is approximately 0 (as are the mean and standard deviation, see Table 3), indicating that the statistical features of the original data and their respective synthetic counterparts are nearly identical. However, some biases can be identified, particularly in the time series generated by the **AR2**, **ARFIMA**, and **HMM** models. Thus, accurately replicating the specific properties exhibited by these time series models is challenging for the *InvQG* method. In fact, the **AR2** model considered here, simulates time series with pseudo-periodic cycles (produced by negative effect) and strong correlations at the first two lags (as illustrated in the corresponding autocorrelation function, ACF, plot in Figure 6a). However, since the Markov process implemented in *InvQG* is only of first order, it cannot fully capture the cycle behavior. At each time step, the choice of the next timestamp depends only on the immediately preceding one. As a result, the synthetic counterpart exhibits a stronger and more persistent autocorrelation and does not exhibit a perfect cyclical pattern as observed in the ACF of the original time series, as seen in Figure 6a. Furthermore, synthetic data exhibits more variability in its dynamic behavior, as seen by the differences in *linearity* and *curvature* (see Figure 4) and in the plots of Figure 6b.

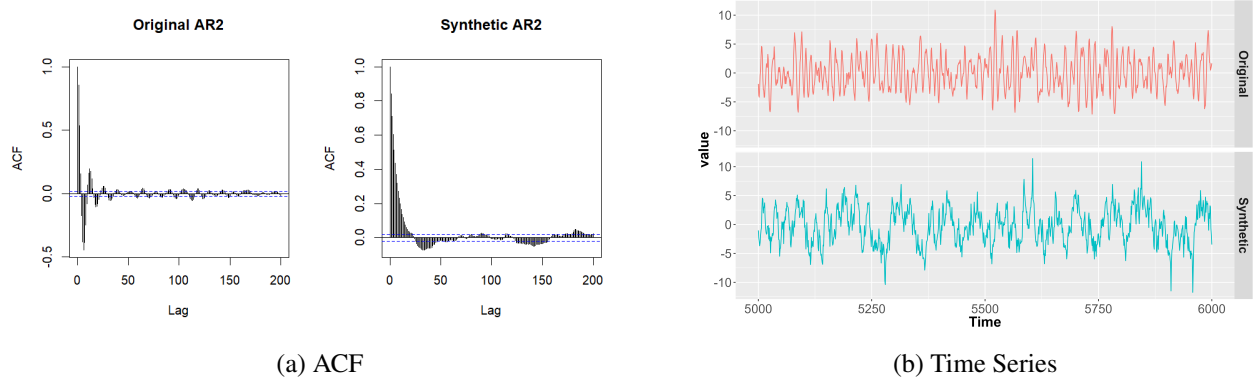


Figure 6: (a) Autocorrelation function (ACF) plot of an original **AR2** time series instance and its synthetic counterpart. (b) Comparison of an original and synthetic time series instance for **AR2** model, only 1000 points shown for clarity.

Similar to **AR2**, **ARFIMA** models are persistent time series with long-range correlation. However, **ARFIMA** time series exhibit a slower decay due to fractional memory. This behaviour is reproduced by its synthetic counterpart, albeit with some differences (see Figure 18a). The synthetic time series generated by *InvQG* exhibits a slower but constant decay, which slightly differs from the original time series. This discrepancy results in a larger difference in features related to autocorrelation properties (see Figure 5).

The time series from the **HMM** model also exhibits persistence, with data states tending to remain unchanged for some time before transitioning to another state (see the Markov matrix in Table 1). This leads to stable periods of low and high intensity, though the synthetic counterparts show slightly less persistence, as seen in the corresponding ACF (Figure 7a) and the differences in lag-10 autocorrelation properties (Figure 5). However, when a state change occurs, there is a sudden shift in the mean of observed values (from 10 to 15 or vice versa), this behaviour is present and can be observed in both the original and synthetic time series (see Figure 7b).

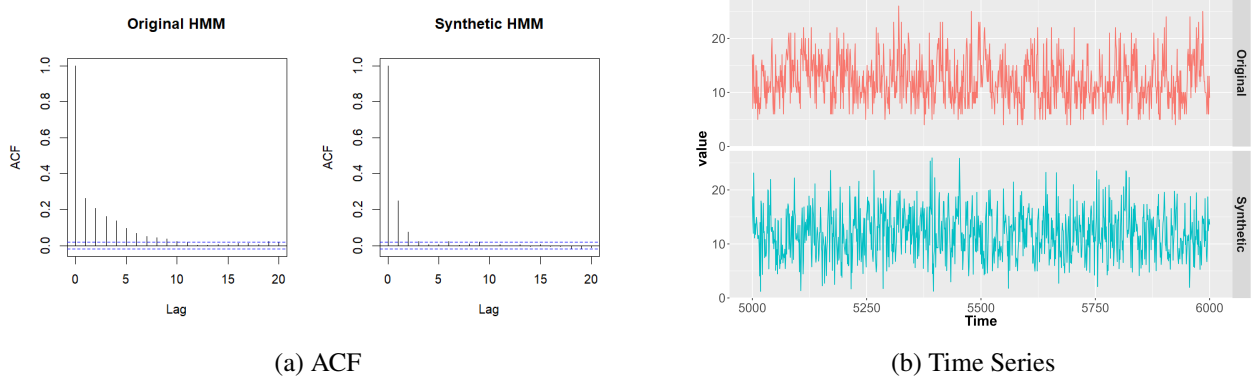


Figure 7: (a) Autocorrelation function (ACF) plot of an original **HMM** time series instance and its synthetic counterpart. (b) Comparison of an original and synthetic time series instance for **HMM** model, only 1000 points shown for clarity.

In general, the presented synthesizing process effectively captures and preserves *trend* behaviour in synthetic time series data. It maintains trend-free characteristics for models with low or no trend, while accurately replicating high-trend patterns in the corresponding synthetic counterparts. Figure 8 shows a comparison of an original and synthetic time series instance for **ARIMA** and **ARFIMA** models.

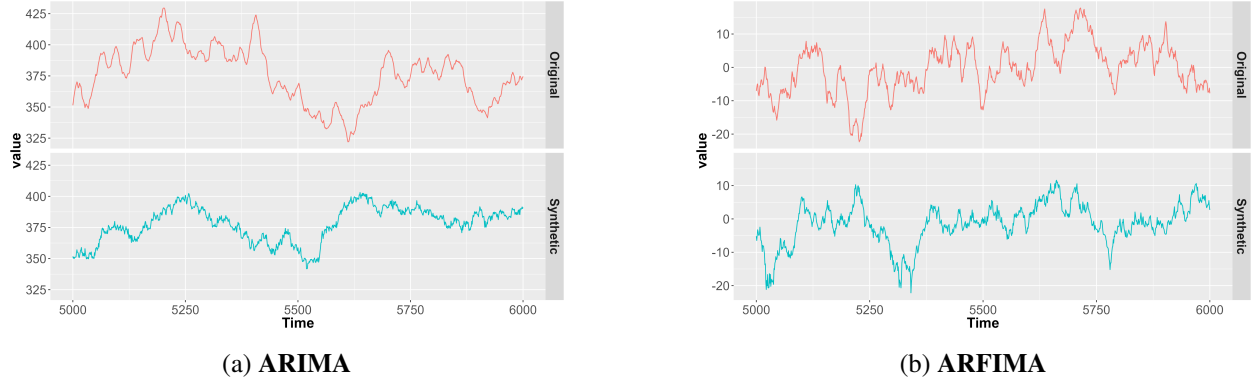


Figure 8: Comparison of an original and synthetic time series instance for (a) **ARIMA** and (b) **ARFIMA** models. Only 1000 points are shown for clarity.

The *entropy* measures the randomness or unpredictability in a time series. Higher values suggest more randomness, while lower values indicate greater predictability and structure. Overall, the *InvQG* method slightly amplifies randomness for all time series models, but it reduces entropy slightly for **AR2** and **ARFIMA** models. As previously analysed, the corresponding synthetic series exhibit a smoother decay in ACF compared to their original counterparts.

Regarding the autocorrelation measures (at lag 1 and 10) of the time series and their first and second differences, *InvQG* successfully maintained values similar to the original counterparts for most time series models, especially those with little or no long-term dependencies. This suggests that, as predicted, *InvQG* effectively captures the immediate relationships between consecutive observations, with the short-term structure of time dependence being well preserved across the series. However, as discussed above, we observe discrepancies in the lag 10 autocorrelation measures and the autocorrelations of the differences, indicating that the long-

term dependence structure is not as well preserved. This can be attributed to the use of only one version of *Quantile Graph* – specifically, the lag 1 version. *InvQG* predominantly captures short-term dependencies, potentially altering the behaviour of the series at more subtle levels by focusing on lag 1 probability transitions, thus neglecting or modifying the long-term serial dependence.

To evaluate the utility of the *InvQG* method, we summarize the set of statistical features explored so far for all time series models using a PCA procedure to analyse the grouping patterns of the time series data. Figure 9 presents the resulting PCA plot for the first two principal components (PCs) explaining 67.7% of the variance. We observe that each time series model tends to form its distinct cluster. In general, the original and synthetic data from the same model are grouped and remain separate from other models. However, in some cases – such as **ARIMA**, **ARFIMA**, **AR2**, and **HMM** models – the original and synthetic samples form separate but closely positioned groups. Additionally, the statistical features that best characterize the original data are the same ones that best describe their synthetic counterparts (see arrows in Figure 9), which shows the preservation of statistical properties of the original data in their synthetic counterparts.

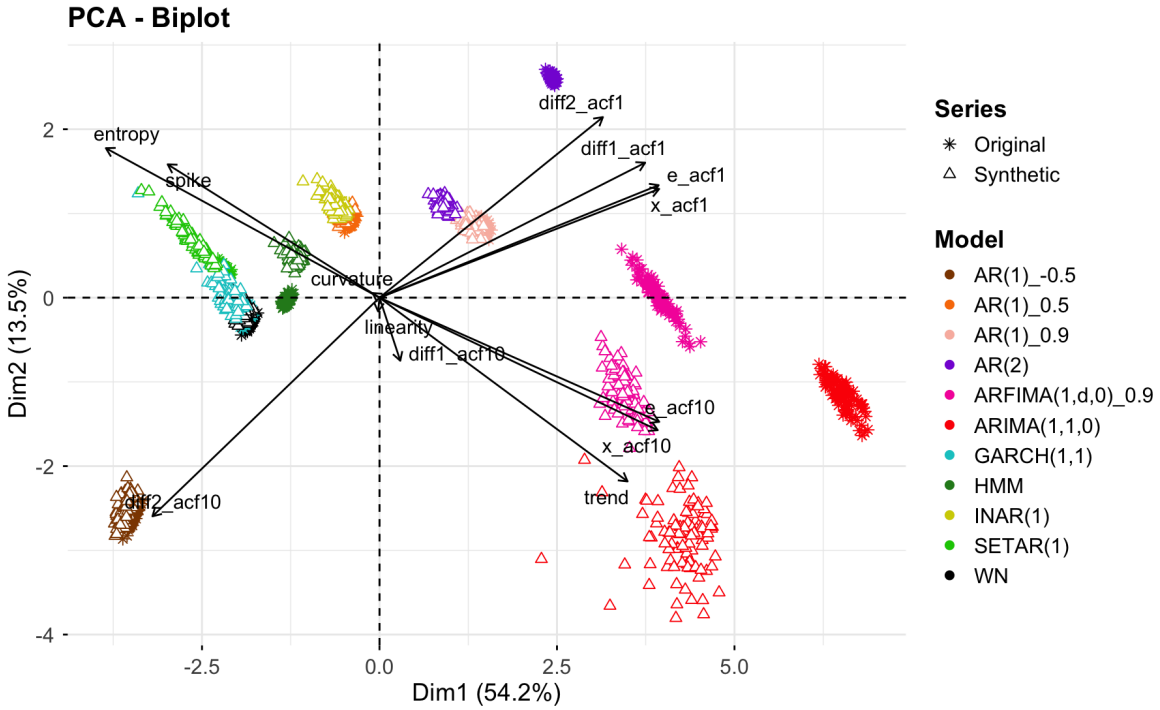


Figure 9: Plot of the first two principal components (PCs) for the original and synthetic time series data. Each time series model is represented by a different color, with original data shown as asterisks and synthetic data as triangles. The arrows indicate the contribution of the corresponding statistical features (*tsfeatures*) to the PCs, the larger the arrow, the greater the feature's contribution.

We were able to identify and clearly distinguish the eleven different time series models and observed a significant proximity between the original samples and the corresponding synthetic samples. This suggests that the original and synthetic data share fundamental similarities and the data utility remains high. Therefore, the *QG*-based method effectively captures essential properties including short-term temporal correlations. However, as analysed above, in some cases it may struggle to capture long-term temporal dependencies, resulting in synthetic data that tend to be more linear when compared to their original counterparts.

4.4 Comparing with Benchmark Methods

In this Section, we benchmark the *InvQG* method against *TimeGAN* and *DoppelGANger* methods. We start by compare the different methods on the *artificial dataset* and then on the *real dataset*.

4.4.1 Artificial Dataset

From the artificial dataset, for each of the different statistical model, we select one time series instance and its respective synthetic version generated using the *InvQG*. Additionally, from each the selected original series we generate two additional synthetic time series using *TimeGAN* and *DoppelGANger* methods. We then plot t-SNE plots for each time series model and by synthesizing method, allowing us to visually compare the performance of these three synthesizing methods, allowing us to quantify the diversity of synthetic data.

We present the results in Figures 10 and 11. The first row of plots corresponds to QG-based mapping methods, the second row to data generated by *TimeGAN*, and the third row to *DoppelGANger*. Red dots represent a set of observations from the original time series, while blue dots represent their respective synthetic counterparts.

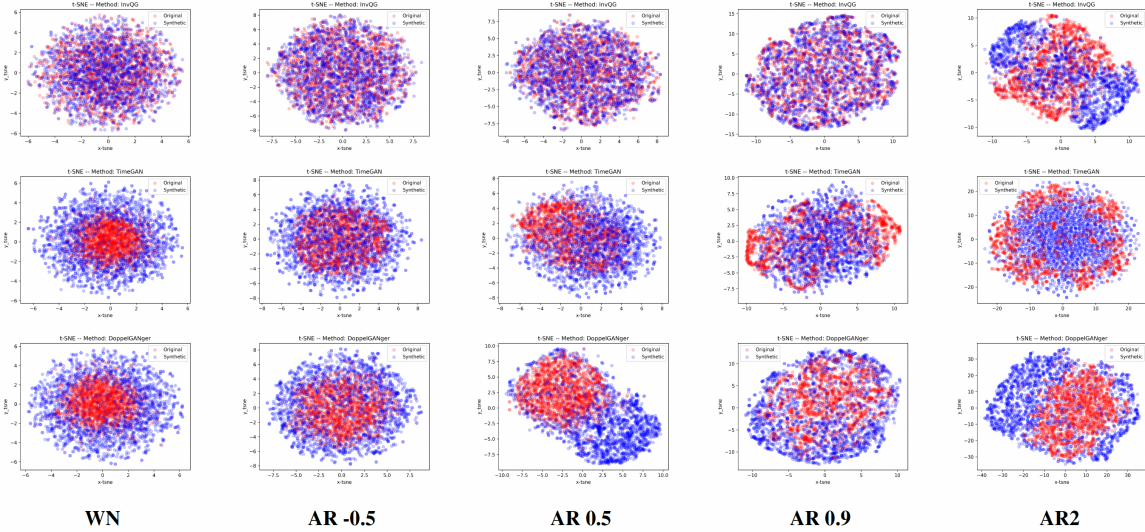


Figure 10: t-SNE comparison between *InvQG* (first row), *TimeGAN* (second row) and *DoppelGANger* (third row) methods for **WN**, **AR -0.5**, **AR 0.5**, **AR 0.9** and **AR2** models.

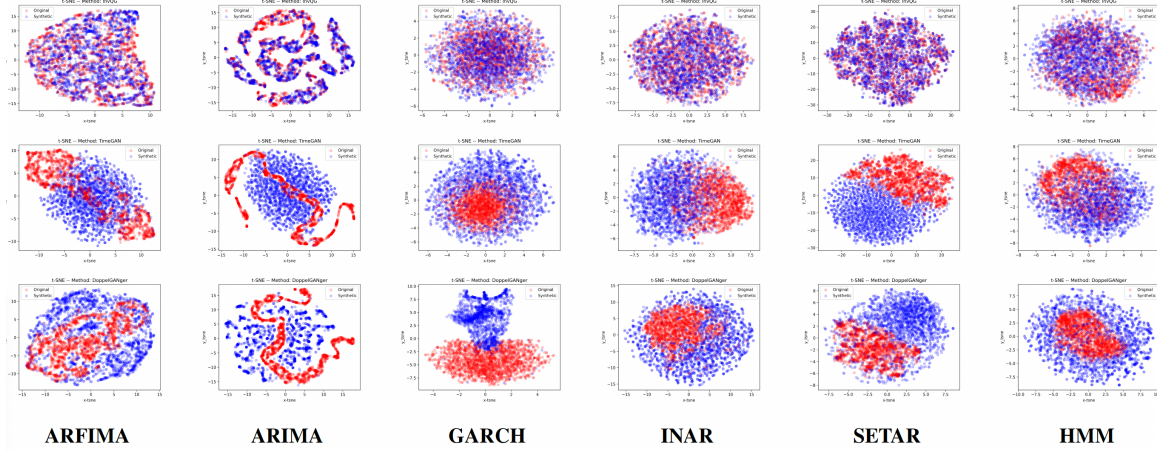


Figure 11: (continued) t-SNE comparison between *InvQG* (first row), *TimeGAN* (second row) and *DoppelGANger* (third row) methods for **ARFIMA**, **ARIMA**, **GARCH**, **INAR**, **SETAR** and **HMM** models.

Based on the t-SNE visualizations, we observe notable differences in the ability of each method to generate synthetic time series that closely resemble the original data. The *InvQG* method demonstrates a similar distribution pattern of original (red) and synthetic (blue) data points across most models, suggesting a strong capacity to preserve the statistical and dynamical properties of the original series. Furthermore, it presents a greater diversity, making it potentially more versatile and useful when compared with the two GAN-based methods. The exception is the model **AR2**, for the reasons discussed in previous sections. In contrast, *TimeGAN* and *DopplerGANger* present an overall difference in distribution and clustering patterns, where the original and synthetic data do not fully overlap and behave differently, indicating potential challenges in capturing certain characteristics from the original time series.

4.4.2 Real Dataset

In this section, we compare the three methods for synthetic time series generation using the 22 real-world time series dataset introduced in Section 4.2.2. For each of the 22 series, we generate three synthetic time series data using the three methods: *InvQG*, *TimeGAN* and *DopplerGANger*.

Figure 12 displays t-SNE plots for 6 representative houses from the dataset (refer to Appendix D for the remaining plots). Each column corresponds to a different house, while each row illustrates the t-SNE plots of the synthetic time series produced by one of the three methods. Consistent with the previous analysis, red dots denote observations from the original time series, and blue dots represent the corresponding synthetic data.

Upon qualitative analysis, we observe that *InvQG* and *DopplerGANger* are the best-performing synthesizers, whereas *TimeGAN* generally struggles to capture the original data distribution across most houses. *InvQG* consistently demonstrates strong similarity between the original and synthetic data for all houses. In contrast, *DopplerGANger* shows limitations in the data of houses 6, 7, 8, 14, 16, and 17.

Among the three synthesis methods, *InvQG* exhibits the best overall performance in capturing and "mimicking" the distribution of the original data. This suggests that, despite its simplicity and previously discussed limitations, *InvQG* is a competitive and effective approach – surpassing even GAN-based methodologies – and represents a viable option for synthetic time series generation.

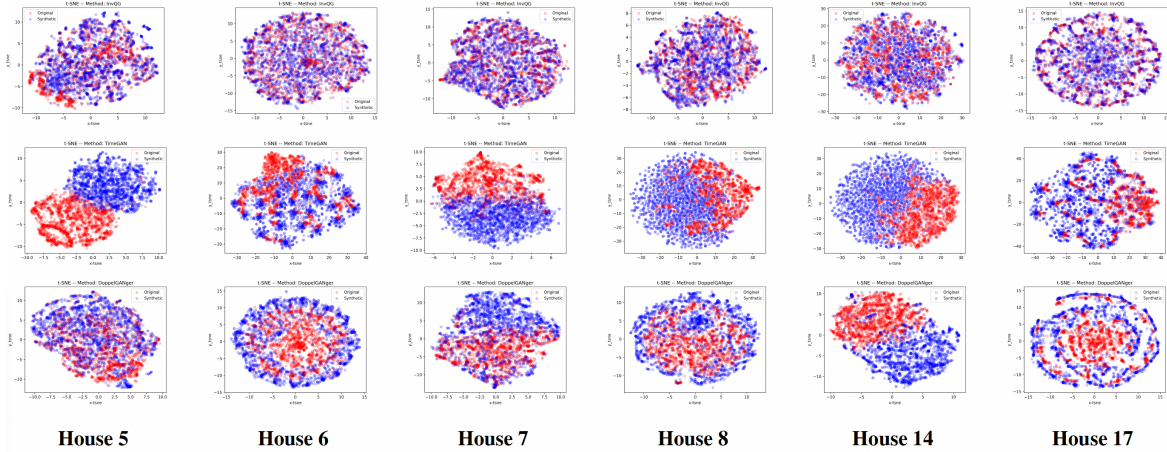


Figure 12: t-SNE comparison between *InvQG* (first row), *TimeGAN* (second row) and *DoppelGANger* (third row) methods for the smart meters of houses 5, 6, 7, 8, 14, and 17 (see Appendix D for remaining houses).

4.5 Utility Analysis via Topological Network Features

In this section, we analyse the similarity between the original time series data and the synthetic series generated by *InvQG*, focusing on their representation as complex networks. Specifically, we assess the resemblance between networks constructed from synthetic time series and those derived from the corresponding original data. To perform this analysis, we employ the *NetF* methodology [Silva et al., 2022], which maps time series into three types of complex networks: the weighted natural visibility graph (WNVG), the weighted horizontal visibility graph (WHVG), and the quantile graph (QG). From each of these networks, *NetF* extracts a vector of fifteen topological features that characterize the data.

Building upon the fidelity analysis presented in Section 4.3, we now evaluate the utility of the proposed QG-based synthetic time series generator. Since the *NetF* feature vector can be applied to a wide range of time series mining tasks – such as clustering, as demonstrated in [Silva et al., 2022] – we analyse the topological network features extracted from the artificial dataset. This analysis includes both the original data and its synthetic counterparts, generated by *InvQG*, using the *NetF* framework.

4.5.1 Graph Features Analysis.

Figure 13 shows the resulting PCA plot of the first two PCs derived from the *NetF* for both original and synthetic data. These two PCs explain 63.4% of the total variance. The overall results are consistent with those obtained using statistical features (Figure 9). The PCA visualization also clearly distinguishes the eleven different time series models. Notably, the **ARIMA**, **AR2** and **HMM** models exhibit some separation between synthetic and original samples, although the synthetic data remains closely clustered within the same model group. Interestingly, for the **ARFIMA** model, the topological features indicate that the original and synthetic data are grouped together, contrasting with the separation observed when using statistical features.

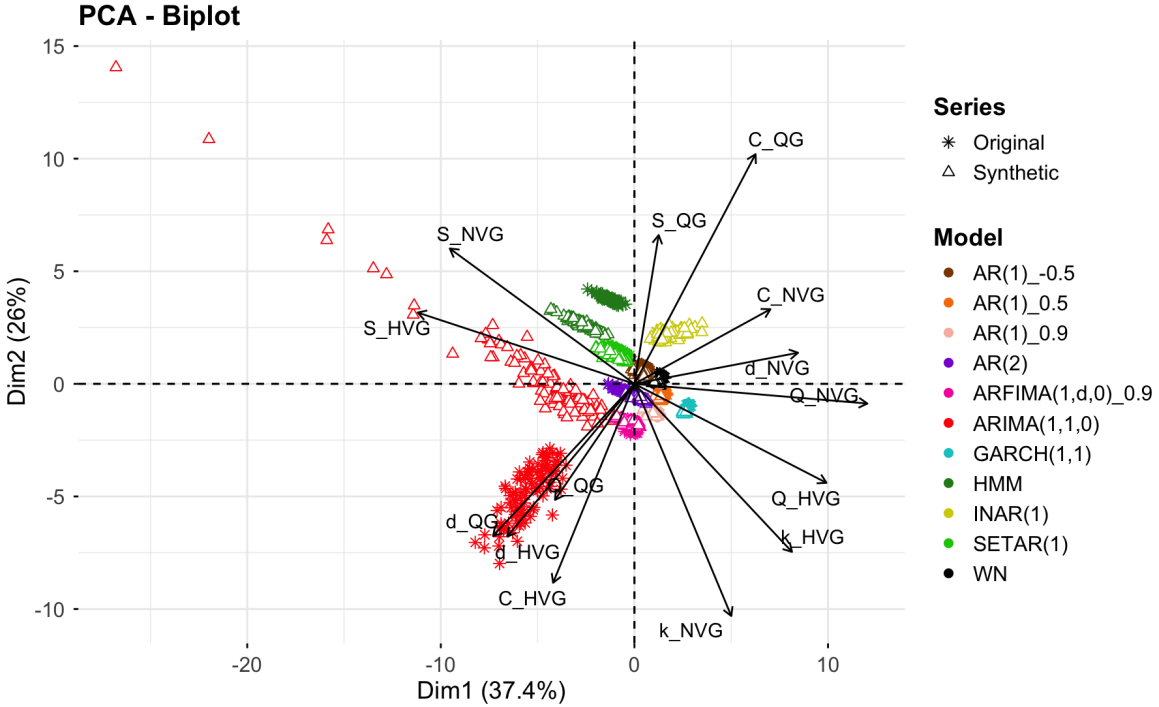


Figure 13: Plot of the first two principal components (PCs) for the original and synthetic time series network data. Each time series model is represented by a different color, with original data shown as asterisks and synthetic data as triangles. The arrows indicate the contribution of the corresponding topological features (*NetF*) to the PCs, the larger the arrow, the greater the feature’s contribution.

A close analysis of modularity (Q) and average average degree (\bar{k}) suggest that synthetic networks successfully captured these topological characteristics from original networks. However, it is also a clear separation between the original and synthetic networks of some time series models (such as **ARIMA**). This indicates that some topological characteristics were not fully captured, such as clustering coefficient (C), average path length (\bar{d}) and number of communities (S).

A divergence in the clustering coefficient (C) could suggest that synthetic data had an variability increase in time series data values, or different temporal correlations in resulting synthetic time series data. This is particularly relevant for visibility graphs, where observations with higher values form larger clusters. This causes them to be more sensitive to magnitude or amplitude changes. Data with more variability, or altered temporal correlations, will create different visibility lines and ultimately alter the clustering behavior in resulting synthetic networks.

Q is also prone to high sensitivity to this added variability in data values. Transitions between quantiles for two consecutive data points will occur differently with this type of amplitude or magnitude change. This unavoidably will result in different quantile transitions and therefore potentially creating different directed weighted links. Leading to a slightly different network structure with different transition probabilities, especially in trended series such as **ARIMA**. Consequently, changes in clustering behavior will also naturally affect the number of communities (S) and average path length (\bar{d}) between nodes.

4.5.2 Clustering Analysis.

To complement and finalize our analysis, we employed *NetF* to perform an empirical clustering analysis following the approach described in [Silva et al., 2022]. We concatenated the *NetF* feature vectors obtained from both the original data and their synthetic counterparts, and used the resulting feature representation to perform clustering across a range of possible numbers of clusters $k \in [2, 21]$. The number of distinct time series models (i.e., 11) serves as the ground truth for evaluating the clustering outcomes.

We used the *K-means* algorithm for clustering and three evaluation metrics: the *Average Silhouette Score* (AS), which does not rely on ground truth labels and how well the data points fit within their assigned clusters; and two validation metrics, *Adjusted Rand Index* (ARI) and the *Normalized Mutual Information* (NMI), which compare clustering assignments against the true labels. For each value of k , the clustering procedure was repeated **100 times** to account for the stochastic nature of initialization and potential convergence to local optima.

Then, for each k , we compute the mean ($\text{mean}_{\text{AS}_k}$) and standard deviation std_{AS_k}) of each evaluation metric (AS, ARI, and NMI) across the 100 runs. To identify the most appropriate number of clusters k^* , we select the k value that achieved a high AS score while maintaining low variability, according to the following weighted criterion ³:

$$k^* = \arg_k \max (\text{mean}_{\text{AS}_k} - 0.5\text{std}_{\text{AS}_k}), \quad (1)$$

which captures both clustering performance and robustness.

Table 2 provides further details on the clustering results, including clustering results using statistical features (*tsfeatures*) instead of *NetF*. The results obtained are consistent with expectations. The maximum values of the clustering metrics were not achieved, as the previously observed and analysed differences in the corresponding PCA plots – particularly between the original and synthetic series of the **ARIMA** and **AR2** models – tend to produce separate clusters.

Feature Set	Source Data	Num. of Clusters	AS [-1, 1]	ARI [0, 1]	NMI [-1, 1]
<i>NetF</i>	original + synthetic	$k^* = 13$	0.68 ± 0.02	0.82 ± 0.05	0.92 ± 0.02
	original + synthetic	$k = 11$	0.65 ± 0.02	0.76 ± 0.03	0.88 ± 0.02
	original	$k = 11$	0.69 ± 0.03	0.94 ± 0.05	0.87 ± 0.03
<i>tsfeatures</i>	original + synthetic	$k^* = 11$	0.69 ± 0.02	0.70 ± 0.05	0.84 ± 0.03
	original + synthetic	$k = 11$	0.69 ± 0.02	0.70 ± 0.05	0.84 ± 0.03
	original	$k = 11$	0.77 ± 0.02	0.81 ± 0.05	0.91 ± 0.03

Table 2: Clustering evaluation metrics. The values reflect the mean and the standard deviation of 100 repetitions of the clustering analysis experiments.

Overall, we conclude that, similarly to the previous *tsfeatures* results, synthetic networks partially capture topological properties from original networks. However, due to the sensitive nature of networks mappings, the clusters are not so well defined and apart when compared to plotting time series data. Nonetheless, we can still visibly see distinct clusters for each time series model. This suggests that synthetic data networks also have utility and could potentially be used instead of original data networks.

³The mean silhouette score reflects the overall clustering quality, whereas the standard deviation indicates the stability of the solution — that is, the consistency of results across repeated runs.

5 Conclusions

Time series data is essential for various domains, including finance, healthcare, and industry, yet accessing high-quality datasets remains difficult due to data scarcity and privacy-based concerns. Synthetic time series data plays a crucial role in addressing these challenges. By generating synthetic data that is statistically similar to the original, it becomes possible to enable robust machine learning model development and exploratory analysis without exposing the original data or increasing the number of samples when available datasets available are limited or scarce.

In this work, we explored an approach to synthetic time series generation by leveraging network-based mapping methods. By mapping time series data into complex networks using Quantile Graph (QG), and then generating synthetic series via Inverse Quantile Graph (*InvQG*), we demonstrated a structured and interpretable methodology for synthesizing high-utility time series data. Unlike deep learning-based generative models, such as *TimeGAN* and *DoppelGANger*, our approach provides a more transparent synthesis process that, additionally, seems to present an improvement in the ability of maintaining core statistical and dynamical properties of the original data.

Our empirical evaluation reveals that the QG-based method effectively preserves short-term temporal dependencies and key statistical characteristics across diverse time series models. However, challenges remain in capturing long-range dependencies, particularly in complex models with higher temporal correlations, and in non-stationary data with strong trend and seasonality components. Nevertheless, the findings retain their value, as further evidenced by our clustering analysis, which suggests that the proposed approach satisfies the criteria of fidelity and utility. Additionally, we presented t-SNE visualizations on both artificial and real datasets to qualitatively evaluate the presented approach against benchmark methods. Our evaluation indicates that the QG-based method is capable to generate synthetic data that more closely follow the distributions of original data compared to GAN-based methods.

This work aims to explore the method based on complex networks for the generation of synthetic time series data and focuses on its interpretability and qualitative evaluation of the results. In future work, we intend to improve and expand the presented method in order to combat the limitations of the presented version, as well as evaluate and apply the proposed methodology in data mining problems appropriate to the topic, to perform a more extensive quantitative analysis of the results.

Availability of data and materials

The raw data are available from the corresponding author upon request.

6 Acknowledgments

This work is funded by national funds through FCT – Fundação para a Ciência e a Tecnologia, I.P., under the project 2023.13039.PEX (<https://doi.org/10.54499/2023.13039.PEX>) and the support UID/50014/2025 (<https://doi.org/10.54499/UID/50014/2025>).

References

- [Asghar et al., 2017] Asghar, M. R., Dán, G., Miorandi, D., and Chlamtac, I. (2017). Smart meter data privacy: A survey. *IEEE Communications Surveys & Tutorials*, 19(4):2820–2835.

- [Benhamouda et al., 2016] Benhamouda, F., Joye, M., and Libert, B. (2016). A new framework for privacy-preserving aggregation of time-series data. *ACM Transactions on Information and System Security (TISSEC)*, 18(3):1–21.
- [Brophy et al., 2023] Brophy, E., Wang, Z., She, Q., and Ward, T. (2023). Generative adversarial networks in time series: A systematic literature review. *ACM Computing Surveys*, 55(10):1–31.
- [Campanharo et al., 2020] Campanharo, A. S., Doescher, E., and Ramos, F. M. (2020). Application of quantile graphs to the automated analysis of eeg signals. *Neural Processing Letters*, 52(1):5–20.
- [Campanharo et al., 2011] Campanharo, A. S., Sirer, M. I., Malmgren, R. D., Ramos, F. M., and Amaral, L. A. N. (2011). Duality between time series and networks. *PloS one*, 6(8):e23378.
- [Chowdhury et al., 2019] Chowdhury, M. J. M., Colman, A., Kabir, M. A., Han, J., and Sarda, P. (2019). Continuous authorization in subject-driven data sharing using wearable devices. In *2019 18th IEEE International Conference On Trust, Security And Privacy In Computing And Communications/13th IEEE International Conference On Big Data Science And Engineering (TrustCom/BigDataSE)*, pages 327–333.
- [Gao et al., 2022] Gao, N., Xue, H., Shao, W., Zhao, S., Qin, K. K., Prabowo, A., Rahaman, M. S., and Salim, F. D. (2022). Generative adversarial networks for spatio-temporal data: A survey. *ACM Transactions on Intelligent Systems and Technology (TIST)*, 13(2):1–25.
- [Halder and Newe, 2022] Halder, S. and Newe, T. (2022). Enabling secure time-series data sharing via homomorphic encryption in cloud-assisted iiot. *Future Generation Computer Systems*, 133:351–363.
- [Hu et al., 2020] Hu, Z., Wu, T., Zhang, Y., Li, J., and Jiang, L. (2020). Time series anomaly detection based on graph convolutional networks. In *2020 2nd International Conference on Applied Machine Learning (ICAML)*, pages 138–145. IEEE.
- [Huang et al., 2021] Huang, Y., Mao, X., and Deng, Y. (2021). Natural visibility encoding for time series and its application in stock trend prediction. *Knowledge-Based Systems*, 232:107478.
- [Hyland et al., 2018] Hyland, S. L., Esteban, C., and Rätsch, G. (2018). Real-valued (medical) time series generation with recurrent conditional GANs.
- [Hyndman et al., 2023] Hyndman, R., Kang, Y., Montero-Manso, P., O’Hara-Wild, M., Talagala, T., Wang, E., Yang, Y., Taieb, S. B., Hanqing, C., Lake, D. K., Laptev, N., Moorman, J. R., and Zhang, B. (2023). tsfeatures: Time series feature extraction. Accessed: January 15, 2024.
- [Iglesias et al., 2023] Iglesias, G., Talavera, E., González-Prieto, Á., Mozo, A., and Gómez-Canaval, S. (2023). Data augmentation techniques in time series domain: a survey and taxonomy. *Neural Computing and Applications*, 35(14):10123–10145.
- [Iwana and Uchida, 2021] Iwana, B. K. and Uchida, S. (2021). An empirical survey of data augmentation for time series classification with neural networks. *Plos one*, 16(7):e0254841.
- [Kang et al., 2020] Kang, Y., Hyndman, R. J., and Li, F. (2020). GRATIS: Generating time series with diverse and controllable characteristics. *Statistical Analysis and Data Mining: The ASA Data Science Journal*, 13(4):354–376.

- [Kegel et al., 2018] Kegel, L., Hahmann, M., and Lehner, W. (2018). Feature-based comparison and generation of time series. In *Proceedings of the 30th international conference on scientific and statistical database management*, pages 1–12.
- [Kingma et al., 2013] Kingma, D. P., Welling, M., et al. (2013). Auto-encoding variational bayes.
- [Klopries and Schwung, 2024] Klopries, H. and Schwung, A. (2024). ITF-GAN: Synthetic time series dataset generation and manipulation by interpretable features. *Knowledge-Based Systems*, 283:111131.
- [Lacasa et al., 2008] Lacasa, L., Luque, B., Ballesteros, F., Luque, J., and Nuno, J. C. (2008). From time series to complex networks: The visibility graph. *Proceedings of the National Academy of Sciences*, 105(13):4972–4975.
- [Leukam Lako et al., 2021] Leukam Lako, F., Lajoie-Mazenc, P., and Laurent, M. (2021). Privacy-preserving publication of time-series data in smart grid. *Security and Communication Networks*, 2021(1):6643566.
- [Lin et al., 2019] Lin, Z., Jain, A., Wang, C., Fanti, G., and Sekar, V. (2019). Generating high-fidelity, synthetic time series datasets with doppelganger. *arXiv preprint arXiv:1909.13403*.
- [Lin et al., 2020] Lin, Z., Jain, A., Wang, C., Fanti, G., and Sekar, V. (2020). Using gans for sharing networked time series data: Challenges, initial promise, and open questions. In *Proceedings of the ACM Internet Measurement Conference*, pages 464–483.
- [Negra et al., 2008] Negra, N. B., Holmstrøm, O., Bak-Jensen, B., and Sørensen, P. (2008). Model of a synthetic wind speed time series generator. *Wind Energy: An International Journal for Progress and Applications in Wind Power Conversion Technology*, 11(2):193–209.
- [Pezoulas et al., 2024] Pezoulas, V. C., Zaridis, D. I., Mylona, E., Androutoss, C., Apostolidis, K., Tachos, N. S., and Fotiadis, D. I. (2024). Synthetic data generation methods in healthcare: A review on open-source tools and methods. *Computational and structural biotechnology journal*, 23:2892–2910.
- [Richardson and Thomson, 2010] Richardson, I. and Thomson, M. (2010). One-minute resolution domestic electricity use data, 2008-2009. <http://doi.org/10.5255/UKDA-SN-6583-1>. [data collection].
- [Roman, 2023] Roman, A.-S. (2023). Evaluating the privacy and utility of time-series data perturbation algorithms. *Mathematics*, 11(5):1260.
- [Shi et al., 2011] Shi, E., Chan, H., Rieffel, E., Chow, R., and Song, D. (2011). Privacy-preserving aggregation of time-series data. In *Annual Network & Distributed System Security Symposium (NDSS)*. Internet Society.
- [Silva et al., 2021] Silva, V. F., Silva, M. E., Ribeiro, P., and Silva, F. (2021). Time series analysis via network science: Concepts and algorithms. *Wiley Interdisciplinary Reviews: Data Mining and Knowledge Discovery*, 11(3):e1404.
- [Silva et al., 2022] Silva, V. F., Silva, M. E., Ribeiro, P., and Silva, F. (2022). Novel features for time series analysis: a complex networks approach. *Data Mining and Knowledge Discovery*, 36(3):1062–1101.

- [Silva et al., 2025] Silva, V. F., Silva, M. E., Ribeiro, P., and Silva, F. (2025). Multilayer quantile graph for multivariate time series analysis and dimensionality reduction. *International Journal of Data Science and Analytics*, 20(3):1795–1807.
- [Wen et al., 2021] Wen, Q., Sun, L., Yang, F., Song, X., Gao, J., Wang, X., and Xu, H. (2021). Time series data augmentation for deep learning: A survey. In *Proceedings of the Thirtieth International Joint Conference on Artificial Intelligence, IJCAI-21*, pages 4653–4660. Survey Track.
- [Yoon et al., 2019] Yoon, J., Jarrett, D., and Van der Schaar, M. (2019). Time-series generative adversarial networks. In Wallach, H., Larochelle, H., Beygelzimer, A., d'Alché-Buc, F., Fox, E., and Garnett, R., editors, *Advances in neural information processing systems*, volume 32.

A Mapping Algorithms

Algorithm 1 Quantile Graph (*Source: Adapted from [Silva et al., 2025])*

Input: time series \mathbf{Y} and number of quantiles \mathcal{Q}
Output: Markov transition matrix \mathbf{W} and the sample quantiles *quantiles*
quantile calculates the range of quantiles from time series support
index_of finds the quantile of a given value

```

1: procedure QG( $\mathbf{Y}, \mathcal{Q}$ )
2:    $\mathbf{W} \leftarrow \text{Array}(\mathcal{Q}, \mathcal{Q})$ 
3:    $quantiles \leftarrow \text{Array}(\mathcal{Q})$ 
4:    $q \leftarrow \text{Array}(\mathcal{Q})$ 
5:   for  $i \leftarrow 1$  to  $\mathcal{Q}$  do
6:      $quantiles[i] \leftarrow i/\mathcal{Q}$ 
7:   end for
8:    $q \leftarrow \text{quantile}(\mathbf{Y}, quantiles)$ 
9:   for  $i \leftarrow 1$  to  $\text{size}(\mathbf{Y}) - 1$  do
10:     $vi \leftarrow \text{index\_of}(\mathbf{Y}[i], q)$ 
11:     $vj \leftarrow \text{index\_of}(\mathbf{Y}[i + 1], q)$ 
12:     $\mathbf{W}[vi][vj] \leftarrow \mathbf{W}[vi][vj] + 1$ 
13:  end for
14:  for  $i \leftarrow 1$  to  $\mathcal{Q}$  do
15:     $sum \leftarrow 0$ 
16:    for  $j \leftarrow 1$  to  $\mathcal{Q}$  do
17:       $sum \leftarrow sum + \mathbf{W}[i][j]$ 
18:    end for
19:    for  $j \leftarrow 1$  to  $\mathcal{Q}$  do
20:       $\mathbf{W}[i][j] \leftarrow \mathbf{W}[i][j]/sum$ 
21:    end for
22:  end for
23:  return  $\mathbf{W}, quantiles$ 
24: end procedure

```

Algorithm 2 Inverse Quantile Graph

Input: time series \mathbf{Y} and number of quantiles \mathcal{Q}
Output: synthetic time series \mathbf{Y}^*
init_sample select randomly sample initial quantile with non-zero probability
runif assign a random value following a uniform distribution in the quantile range
select_next_quantil select next node based on transition probabilities

```
1: procedure INVQG( $\mathbf{Y}, \mathcal{Q}$ )
2:    $\mathbf{W}, \text{quantiles} \leftarrow \text{QG}(\mathbf{Y}, \mathcal{Q})$ 
3:    $T \leftarrow \text{size}(\mathbf{Y})$ 
4:    $\mathbf{Y}^* \leftarrow \text{Array}(T)$ 
5:    $ni \leftarrow \text{init\_sample}(\mathbf{W})$ 
6:   for  $t \leftarrow 1$  to  $T$  do
7:      $\text{min\_range} \leftarrow \text{quantiles}[ni - 1]$ 
8:      $\text{max\_range} \leftarrow \text{quantiles}[ni]$ 
9:      $\mathbf{X}[t] \leftarrow \text{runif}(\text{min\_range}, \text{max\_range})$ 
10:     $ni \leftarrow \text{select\_next\_quantil}(\mathbf{W}[ni])$ 
11:   end for
12:   return  $\mathbf{Y}^*$ 
13: end procedure
```

B Mean and SD Tables of Differences

Table 3: Mean and standard deviation of the paired samples (*synthetic-original*) of statistical features. The values correspond to the mean (and standard deviation) of the 100 instances of each original and synthetic time series models for each feature.

Model	trend	linea.	curvat.	entro.	e_acf1	e_acf10	x_acf1	x_acf10
AR -0.5	-0.000 (0.000)	0.089 (0.778)	0.010 (0.715)	0.001 (0.001)	0.005 (0.009)	-0.004 (0.020)	0.005 (0.001)	-0.004 (0.020)
AR 0.5	0.000 (0.003)	-0.034 (2.536)	-0.020 (2.300)	0.001 (0.001)	-0.004 (0.008)	-0.005 (0.019)	-0.004 (0.008)	-0.005 (0.019)
AR 0.9	0.001 (0.016)	1.117 (5.925)	0.376 (6.212)	0.003 (0.005)	-0.007 (0.005)	-0.088 (0.179)	-0.006 (0.004)	-0.081 (0.187)
AR2	0.023 (0.009)	-0.687 (3.334)	0.133 (3.813)	-0.007 (0.004)	-0.011 (0.005)	0.852 (0.125)	-0.007 (0.005)	0.964 (0.126)
ARFIMA	0.051 (0.097)	-2.396 (29.840)	-1.298 (24.682)	-0.074 (0.0177)	-0.007 (0.003)	0.854 (0.244)	-0.003 (0.001)	0.658 (0.177)
ARIMA	-0.041 (0.086)	5.500 (63.808)	3.799 (60.870)	0.063 (0.108)	-0.042 (0.095)	-1.017 (1.193)	-0.004 (0.009)	-0.130 (0.215)
GARCH	-0.000 (0.001)	0.083 (1.394)	0.079 (1.321)	0.000 (0.000)	-0.000 (0.011)	-0.000 (0.001)	-0.001 (0.011)	-0.000 (0.001)
HMM	-0.006 (0.003)	-0.013 (2.570)	0.021 (2.207)	0.008 (0.001)	-0.004 (0.009)	-0.107 (0.013)	-0.008 (0.009)	-0.120 (0.014)
INAR	-0.000 (0.001)	0.096 (1.987)	0.009 (1.955)	0.000 (0.001)	-0.002 (0.009)	-0.003 (0.018)	-0.003 (0.009)	-0.003 (0.018)
SETAR	0.000 (0.000)	-0.117 (0.939)	-0.062 (0.809)	0.000 (0.000)	-0.012 (0.007)	-0.003 (0.003)	-0.012 (0.007)	-0.003 (0.003)
WN	0.000 (0.001)	-0.303 (1.324)	0.0301 (1.337)	-0.000 (0.000)	0.000 (0.010)	0.000 (0.001)	0.000 (0.010)	0.000 (0.001)

C Simulated Dataset: Original *vs* Synthetic Counterparts

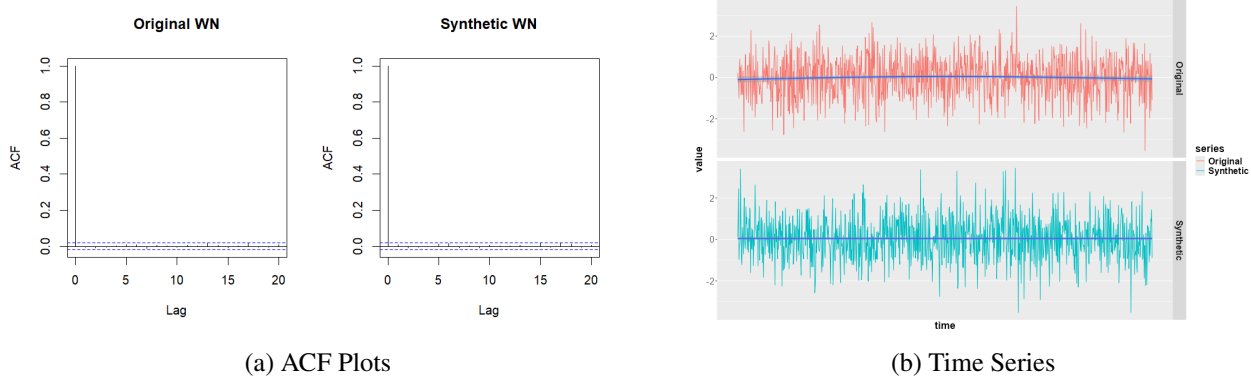


Figure 14: (a) Autocorrelation function (ACF) plot of an original **WN** time series instance and its synthetic counterpart. (b) Comparison of an original and synthetic time series instance for **WN** model, only 1000 points shown for clarity.

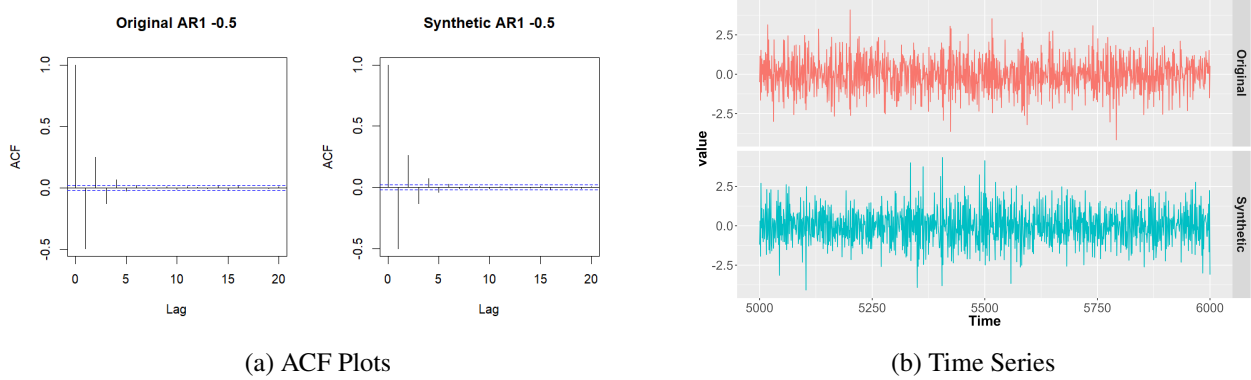


Figure 15: (a) Autocorrelation function (ACF) plot of an original **AR1 -0.5** time series instance and its synthetic counterpart. (b) Comparison of an original and synthetic time series instance for **AR1 -0.5** model, only 1000 points shown for clarity.

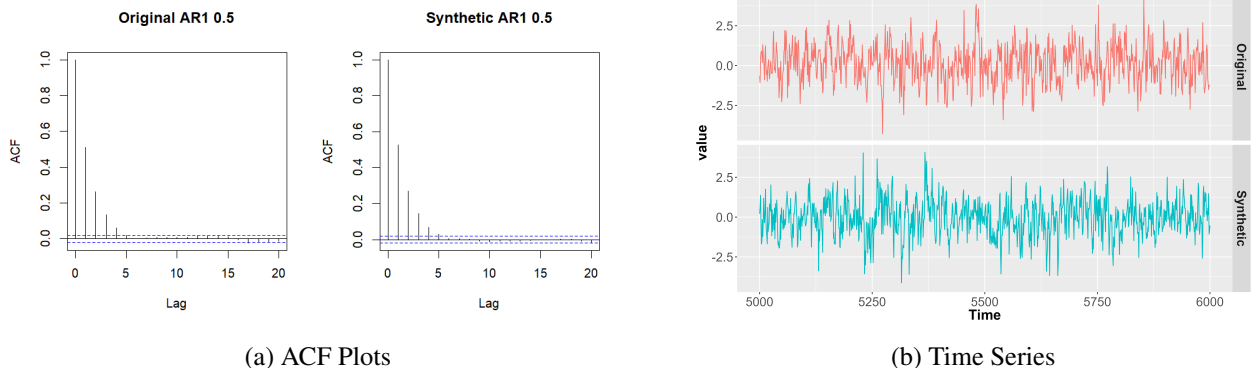


Figure 16: (a) Autocorrelation function (ACF) plot of an original **AR1 0.5** time series instance and its synthetic counterpart. (b) Comparison of an original and synthetic time series instance for **AR1 0.5** model, only 1000 points shown for clarity.

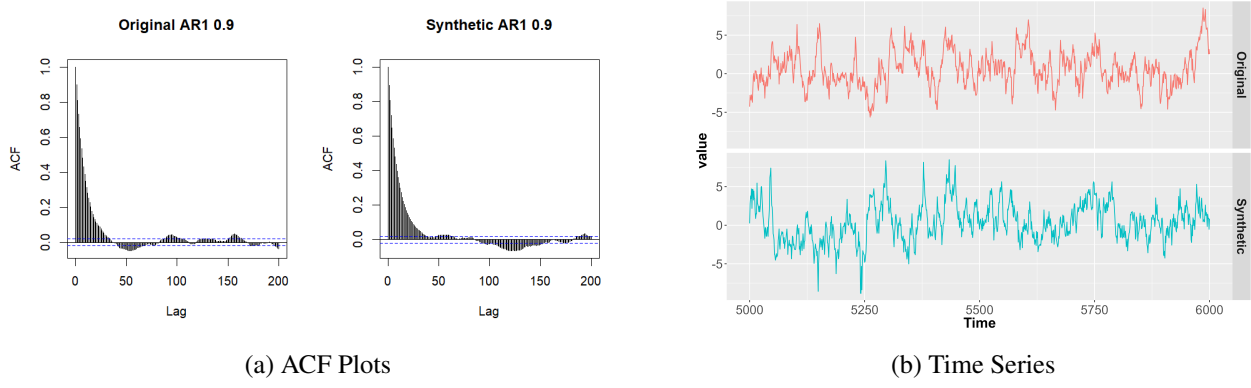


Figure 17: (a) Autocorrelation function (ACF) plot of an original **AR1 0.9** time series instance and its synthetic counterpart. (b) Comparison of an original and synthetic time series instance for **AR1 0.9** model, only 1000 points shown for clarity.

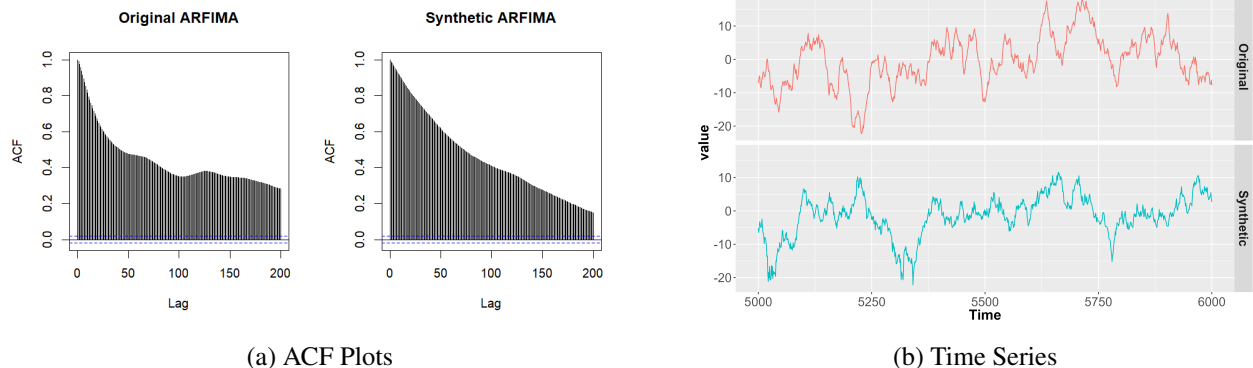


Figure 18: (a) Autocorrelation function (ACF) plot of an original **ARFIMA** time series instance and its synthetic counterpart. (b) Comparison of an original and synthetic time series instance for **ARFIMA** model, only 1000 points shown for clarity.

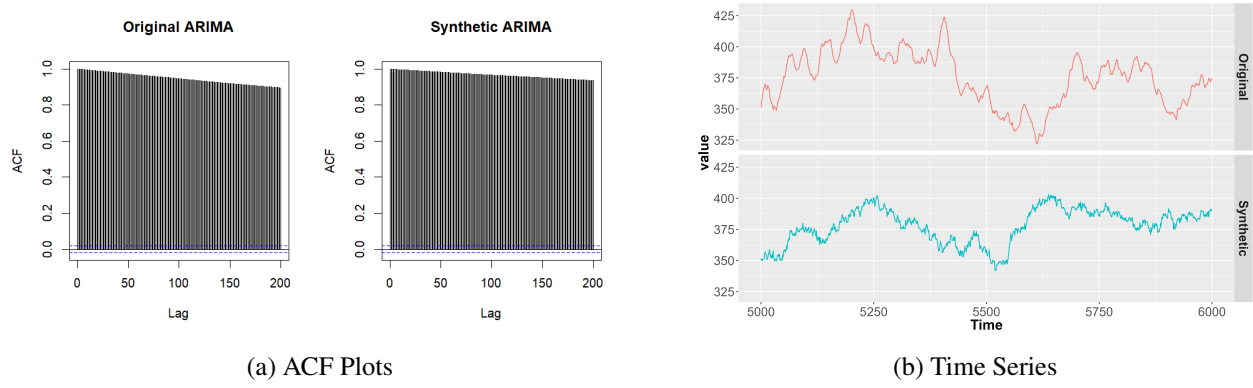


Figure 19: (a) Autocorrelation function (ACF) plot of an original **ARIMA** time series instance and its synthetic counterpart. (b) Comparison of an original and synthetic time series instance for **ARIMA** model, only 1000 points shown for clarity.

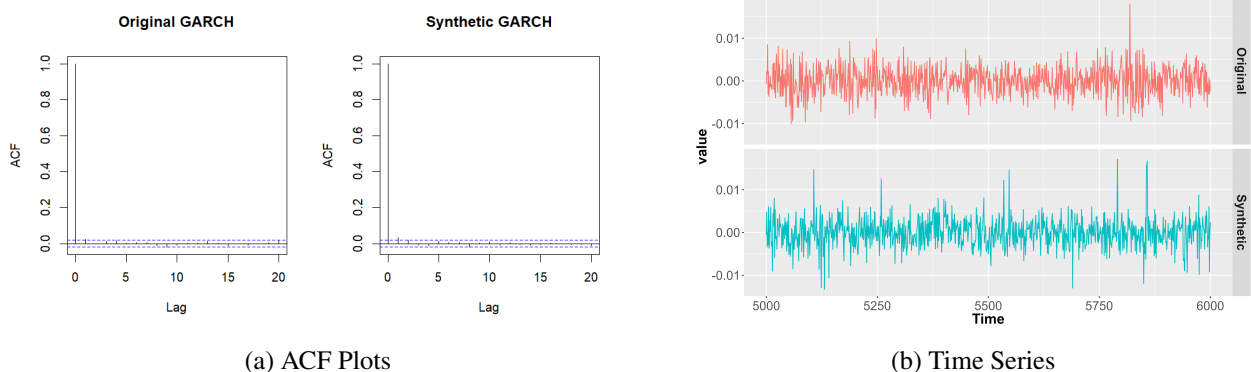


Figure 20: (a) Autocorrelation function (ACF) plot of an original **GARCH** time series instance and its synthetic counterpart. (b) Comparison of an original and synthetic time series instance for **GARCH** model, only 1000 points shown for clarity.

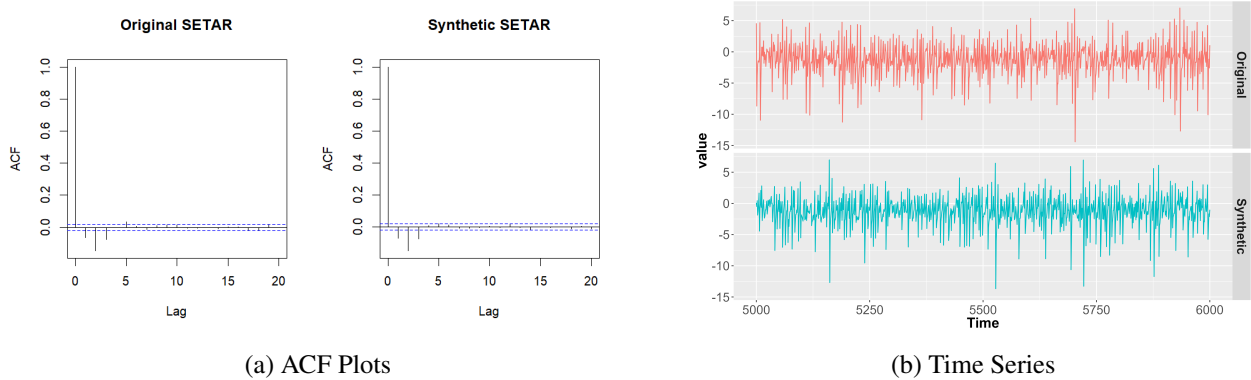
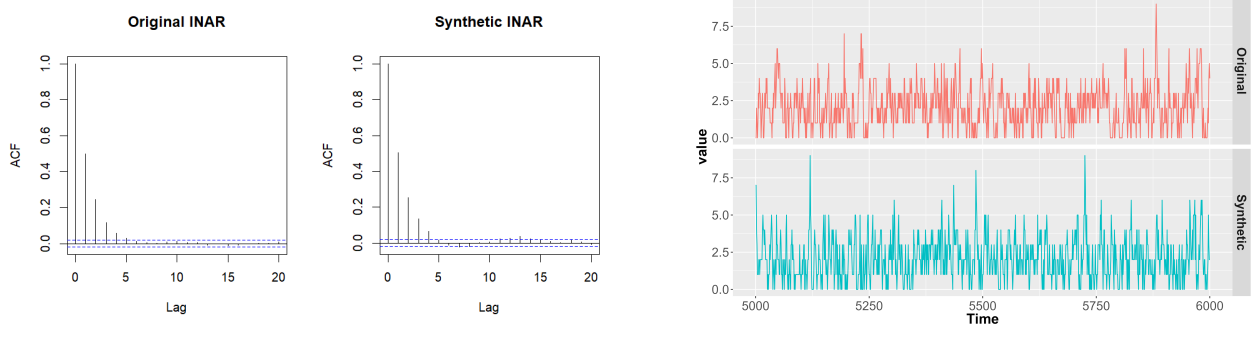


Figure 21: (a) Autocorrelation function (ACF) plot of an original **SETAR** time series instance and its synthetic counterpart. (b) Comparison of an original and synthetic time series instance for **SETAR** model, only 1000 points shown for clarity.



(a) ACF Plots

(b) Time Series

Figure 22: (a) Autocorrelation function (ACF) plot of an original **INAR** time series instance and its synthetic counterpart. (b) Comparison of an original and synthetic time series instance for **INAR** model, only 1000 points shown for clarity.

D Real Dataset: Comparing with Benchmark Methods

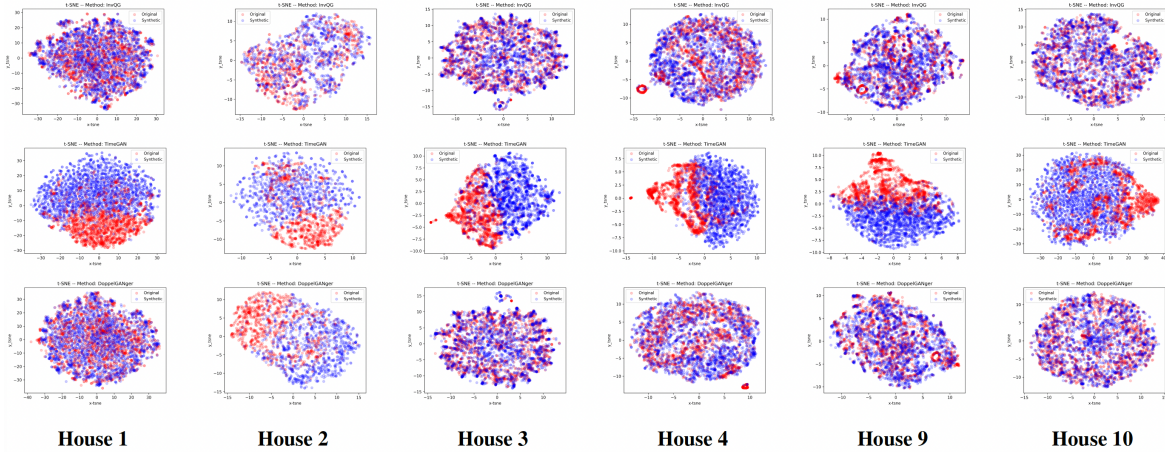


Figure 23: t-SNE comparison between *InvQG* (first row), *TimeGAN* (second row) and *DoppelGANger* (third row) methods for the smart meters of houses 1, 2, 3, 4, 9, and 10 (*continued*).

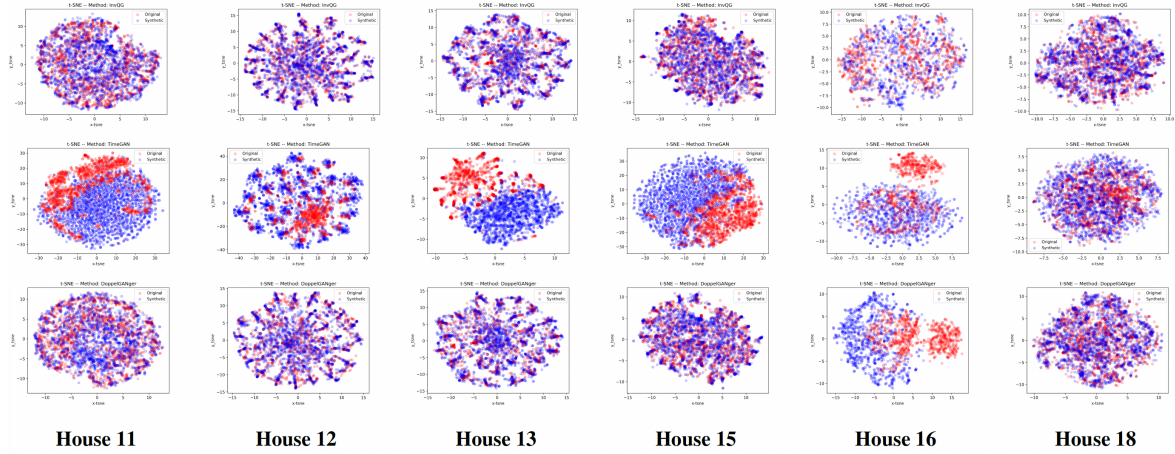


Figure 24: t-SNE comparison between *InvQG* (first row), *TimeGAN* (second row) and *DoppelGANger* (third row) methods for the smart meters of houses 11, 12, 13, 15, 16, and 18 (*continued*).

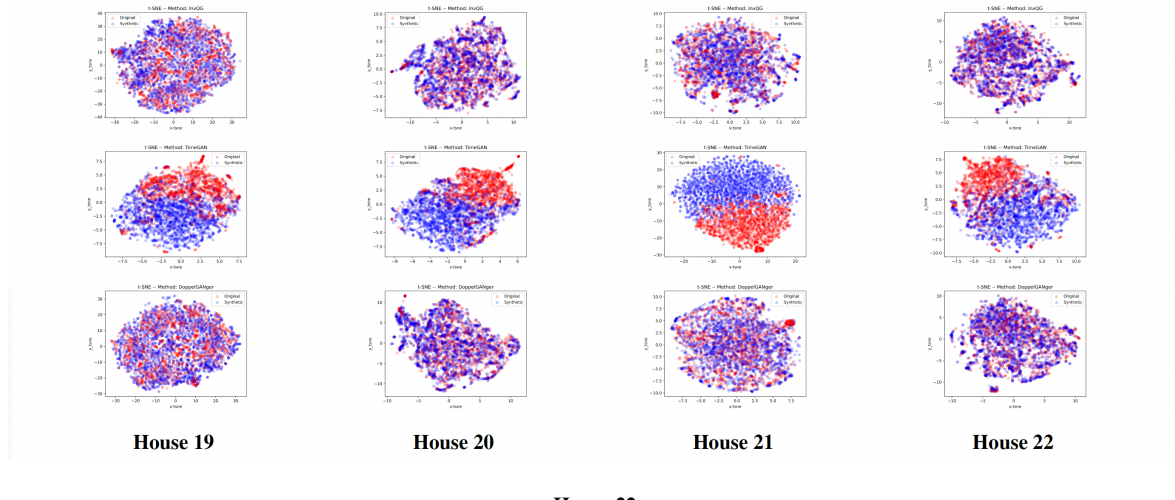


Figure 25: t-SNE comparison between *InvQG* (first row), *TimeGAN* (second row) and *DoppelGANger* (third row) methods for the smart meters of houses 19, 20, 21, and 22 (*continued*).